Experimental and Numerical Studies of an Acoustic Coupler for Multiplexing of Guided Waves for SHM

CAMERON MARASHI, JEE MYUNG KIM and KARA PETERS

ABSTRACT

Optical fibers can propagate both lightwaves and ultrasonic waves, as has been recently shown to be useful for guided wave based SHM. Additionally, the ultrasonic waves can be transferred between optical fibers using an acoustic coupler. This paper discusses the role of geometrical parameters on the acoustic energy transferred between two cylindrical waveguides, through a bonded coupler. Finite element simulations of the energy transfer are performed for different parameter sweeps.

INTRODUCTION

Structural health monitoring (SHM) using guided waves has been broadly applied for thin-walled structures. One of the challenges of this technique is the need to collect the wave packets with sufficient resolution, such that the features can be accurately extracted for damage identification. Using fiber Bragg grating (FBG) sensors, the technique of remote bonding was recently introduced to amplify the extracted signal by first converting the guided waves in the structure into longitudinal acoustic modes in the optical fiber [1,2,3]. Thus the optical fiber acts to transmit both lightwaves and ultrasonic waves. As the ultrasonic waves are of much longer wavelengths, as compared to the diameter of the optical fiber, the thin-rod assumption can be applied to understand the behavior of the longitudinal mode [4]. The longitudinal mode is then detected with a FBG sensor at a distance along the optical fiber.

More recently, it has also been shown that the acoustic modes can be coupled to a second optical fiber through an adhesive bond [5]. This permits multiplexing of signals from different waveguides to a single optical fiber for processing. Additionally, the waveguide coupled to the structure no longer needs to be an optical fiber suitable for FBG writing. This paper presents the role of the acoustic coupler geometry on the signal coupling between two optical fiber waveguides. In addition, finite element numerical simulations of the acoustic wave propagation through the coupler are also presented to both validate the measurements and to perform broader parameter sweeps.

Cameron Marashi, Jee Myung Kim, Kara Peters, Department of Mechanical and Aerospace Engineering, North Carolina State University, Campus Box 7910, Raleigh, NC 27695, U.S.A.

EXPERIMENTAL MEASUREMENT OF COUPLER BEHAVIOR

Experimental measurements of the output to input fiber mode amplitudes for the longitudinal modes were previously performed by Kim et al. [5] varying the input fiber diameter and the input fiber material. Additionally, experiments were performed for hollow, silica input fibers. These experiments used a configuration like the one shown in Figure 1 and were based on manually adhering a small length of the two fibers. The results demonstrated that as the input fiber cross-section increases (holding the output fiber diameter constant), the longitudinal mode amplitude in the output fiber decreases. Additionally the output longitudinal mode amplitude varied with the input fiber material. However two main challenges were identified in evaluating the experimental results: first the experiments were only performed for a few cases and second it was not possible to accurately control the coupler length or adhesive thickness. A modification to the process was developed where the coupler was molded, however the mold release spray interacted with the adhesive and produced inconsistent coupler geometries. An example coupler is shown in Figure 2, stitched together from several microscope images. Therefore, finite element simulations of the coupler behavior were performed to better understand the critical geometric parameters of the bonded coupler. These simulations are described in the following section. In addition, the fabrication process for the coupler is currently being improved, such that better control of the adhesive coupler length and thickness can be achieved.

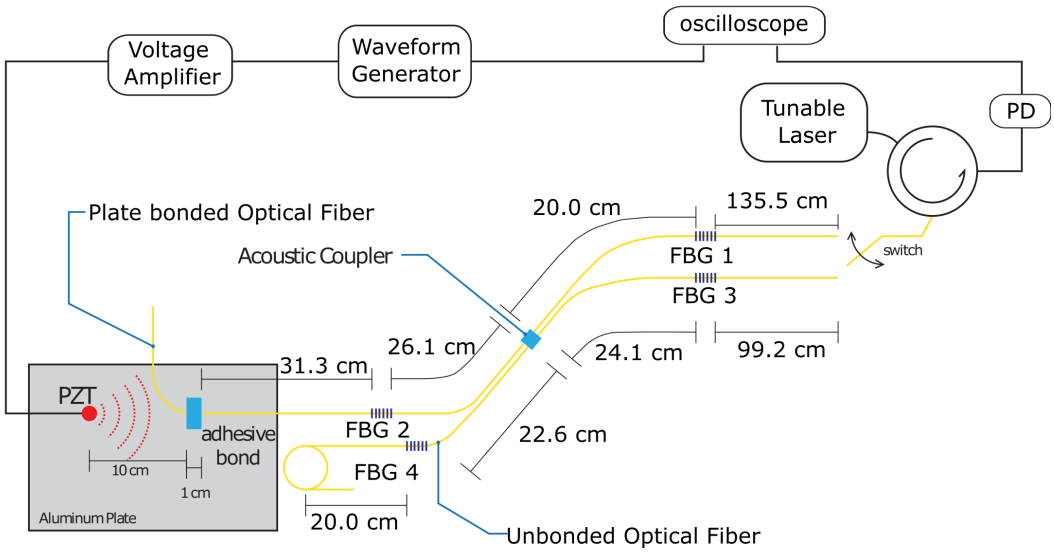

Figure 1. Experimental setup to measure bonded acoustic coupler efficiency. Longitudinal mode in input fiber is generated from S_0 mode in plate at adhesive bond. Both the amplitude of the input mode and the output mode were measured with FBGs 2 and 3 respectively.

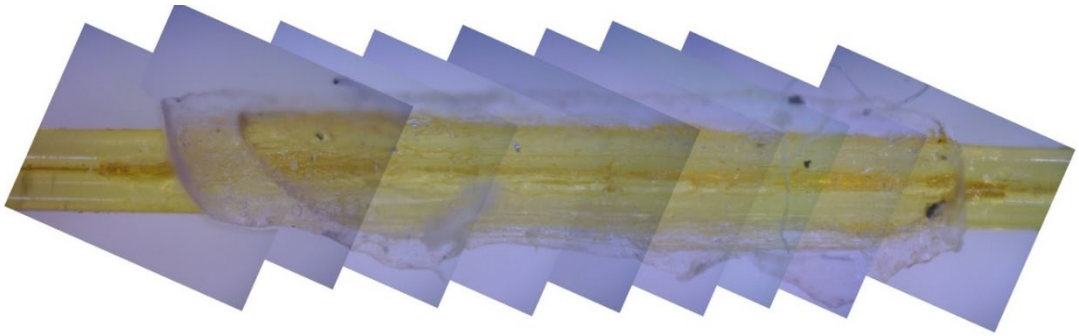

Figure 2. Stitched photograph of the acoustic coupler fabricated using 3 mm stainless steel mold.

SIMULATIONS OF COUPLER BEHAVIOR

To test a wider range of geometric parameters, the coupler was modeled using the finite element software COMSOL acoustics module, as shown in Figure 3. The simulations discretize the inhomogeneous Helmholtz equation for acoustic waves in a lossless medium,

$$\frac{1}{c^2}\frac{\partial^2 p}{\partial t^2} - \nabla \cdot (\nabla \cdot p) = 0 \tag{1}$$

where p is the total pressure, c is the speed of sound in the medium, and t is time [6]. This equation reduces to

$$\nabla \cdot (\nabla p) + \frac{\omega^2}{c^2} p = 0 \tag{2}$$

for harmonic waves where ω is the angular frequency of the wave. One-half of the fiber and coupler geometry was modeled using the plane of symmetry.

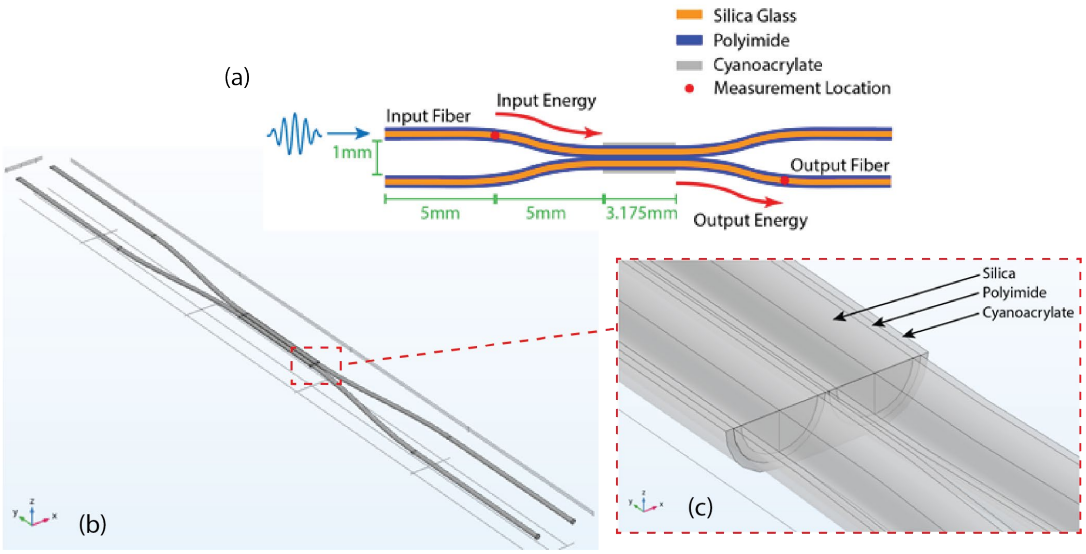

Figure 3. Finite element model of bonded acoustic coupler. (a) Schematic of coupler geometry; (b) COMSOL model; (c) detail of coupler region.

A Hanning windowed tone burst pressure wave was input into the end cross-section of the input fiber and the waveform was measured at a point along the output fiber, as shown in Figure 3(a). The optical fiber is modeled as silica, the fiber coating polyimide and the adhesive cyanoacrylate, to match the previously fabricated couplers. At the output end of the fibers, impedance matching boundary conditions were applied to prevent back-reflected acoustic waves.

Parameter sweeps were performed for the input fiber diameter, output fiber diameter, adhesive length and adhesive thickness. Example outputs are shown in Figure 4 for sweeps of the input and output fiber diameter. In both cases the other fiber diameter is held constant. The results are as expected, because as the fiber cross-section increases, conservation of energy drives that the longitudinal mode amplitude decreases. As the input mode amplitude is kept constant, the output mode amplitude is proportional to the input fiber to output fiber cross-sectional area in the theoretical system. The simulations plotted in Figure 4(a) were then compared to the previous experimental data of Kim et al [5], plotted in Figure 4(c). The trend between the two data sets is the same with fiber cross-sectional area. The exact values of the amplitude ratio are not the same, as the simulations do not include losses and assume a perfect contact between the two fibers. However, these results indicate that the simulations can be used to understand the trends with different geometrical parameters and optimize the coupler geometry. The drop off in amplitude for the largest diameter fiber was also greater for the experiments, most likely because the large mismatch in fiber diameters created a poor adhesive geometry between them, whereas in the simulations the adhesive maintained an ideal shape.

The accuracy of the waveform in the output fiber was also checked, as compared to the original Hanning windowed input. The original Hanning windowed signal can be seen in the input fiber displacement plot in Figure 5(a). For most of the parameter sweeps described above, the waveform was preserved. One exception, however, was when the thickness of the adhesive was significantly increased, as can be seen in the results of Figure 5. For the thinnest adhesive case, shown in Figure 5(a), the output waveform is reduced in amplitude but otherwise replicates the original wave. A similar behavior is observed for the medium thickness case shown in Figure 5(b).

However, for the largest adhesive thickness, shown in Figure 5(c), the window of the waveform is significantly changed. Most likely this distortion is due to resonance effects in the coupler itself. As can be seen in the CAD model of the large adhesive thickness case of Figure 5(c), the mass of the adhesive is much larger than that of the optical fibers themselves. Therefore, the adhesive mass is sufficient to create a discrete, large change in the local acoustic impedance and create a Fabry-Perot interference of the mode between the front and rear edge of the coupler. Although, not plotted here, this behavior could be seen by the changing reflections from the coupler as well.

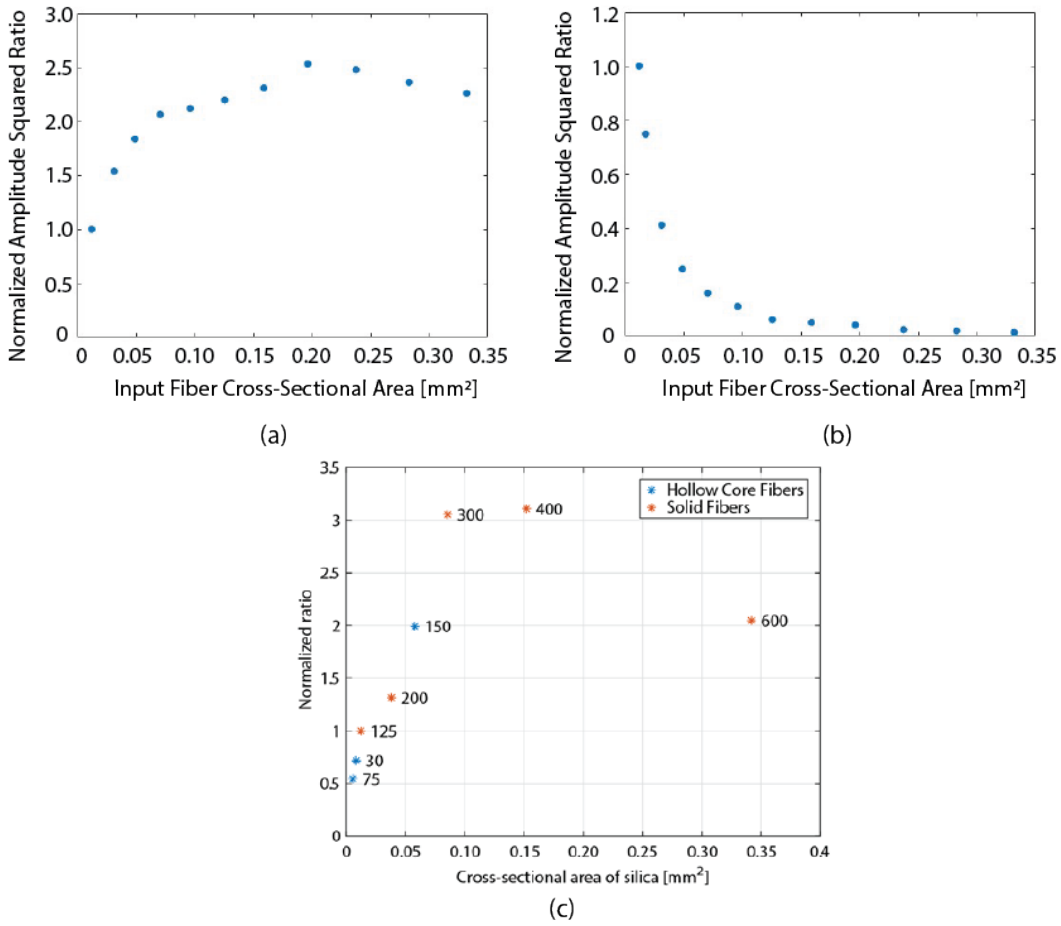

Figure 4. Calculated longitudinal mode amplitudes in output fiber from finite element simulations. (a) Parameter sweep of input fiber diameter. (b) Parameter sweep of output fiber diameter. Amplitude values are normalized to the case where input and output fibers have the same cross-sectional area. (c) Experimental measurements of normalized amplitude of L_{01} mode coupling for solid and hollow core fibers, plotted as a function of cross-sectional area. Labels next to each data point approximate silica diameters. [5].

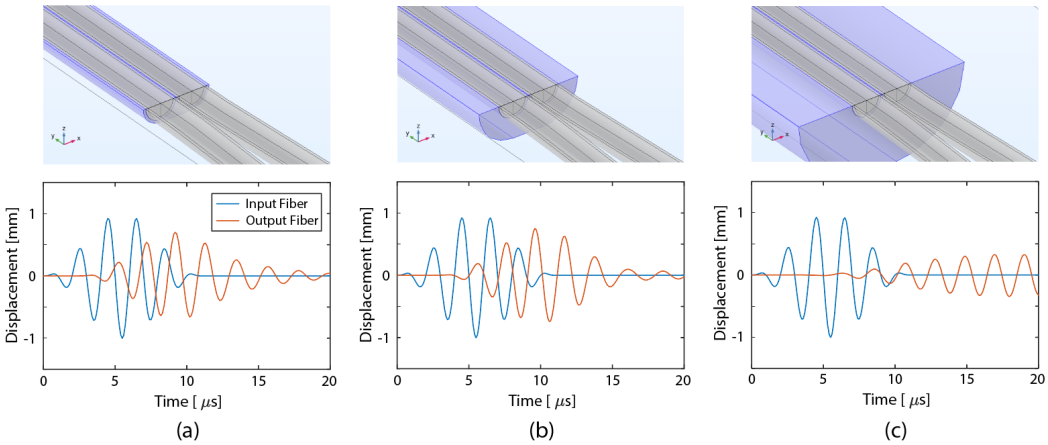

Figure 5. Screenshots and the input and output fiber displacements when the coupler thickness is (a) 12.5μm, (b) 100μm, and (c) 275μm.

CONCLUSIONS

The results demonstrate that the numerical simulations do well predict the coupling behavior of the couplers, at least those previous tested experimentally. Further experiments are needed once the coupler fabrication process has been improved to provide repeatable and controllable adhesive geometries for the coupler. The simulations further reveal that the slight signal distortion of the acoustic wave that is sometimes apparent is due to interference created by the edges of the coupler. Therefore tapering of the coupler would likely reduce the signal distortion. The numerical simulations do not actually predict the loss in signal energy at the location of the coupler, which is a critical factor in optimizing the sensor array for a given application. Therefore, the simulations will be modified to attempt to better capture the loss in the future. Once the coupler efficiency is better understood, in terms of the geometrical parameters, couplers can be designed to couple specific percentages of the input fiber mode energy to one or more output fibers and integrated into SHM optical fiber based sensor networks.

ACKNOWLEDGEMENTS

This work was supported by the US Office of Naval Research (ONR) through grant no. N00014-19-1-2053.

REFERENCES

1. Wee, J., B. Wells, D. Hackney, P. Bradford, and K. Peters. 2016. “Increasing signal amplitude in fiber Bragg grating detection of Lamb waves using remote bonding,” *Appl. Opt.,* 55(21):5564-5569.
2. J. Lee, H. Tsuda. 2006. “Sensor Application of fibre ultrasonic waveguide,” *Meas. Sci. Technol.,* 17(4):645.
3. Lee, J.R., H. Tsuda. 2005. “Fiber optic liquid leak detection technique with an ultrasonic actuator and a fiber Bragg grating,” *Opt. Lett.,* 30(24):3293-3295.
4. Thurston R.N. 1978. “Elastic waves in rods and clad rods,” *J. Acoust. Soc. Am.,* 64(1):1-37.
5. Kim, J.M., C. Marashi, J. Wee, and K. Peters. 2021. “Acoustic wave coupling between optical fibers of different geometries,” *Appl. Opt.,* 60(36):11042.
6. COMSOL Acoustic Module User Manual, Version 5.4, 2018.